Electronic Supplementary Information

Electronic Properties of Graphene Oxide: Nanoroads Towards the Novel Applications

Almaz Khabibrakhmanov[a,b,c*], Pavel Sorokin[a,b,*]

[a] National University of Science and Technology MISiS, 119049, 4 Leninskiy prospekt, Moscow, Russian Federation

[b] Moscow Institute of Physics and Technology (National Research University), 141701, 9 Institutskiy pereulok, Dolgoprudny, Moscow Region, Russian Federation

[c] Department of Physics and Materials Science, University of Luxembourg, L-1511 Luxembourg City, Luxembourg

[*] E-mail addresses: almaz.khabibrakhmanov@phystech.edu, pbsorokin@misis.ru

The presented Electronic Supplementary Material includes the auxiliary and complementary figures with the captions and, where required, with some additional explanation in text.

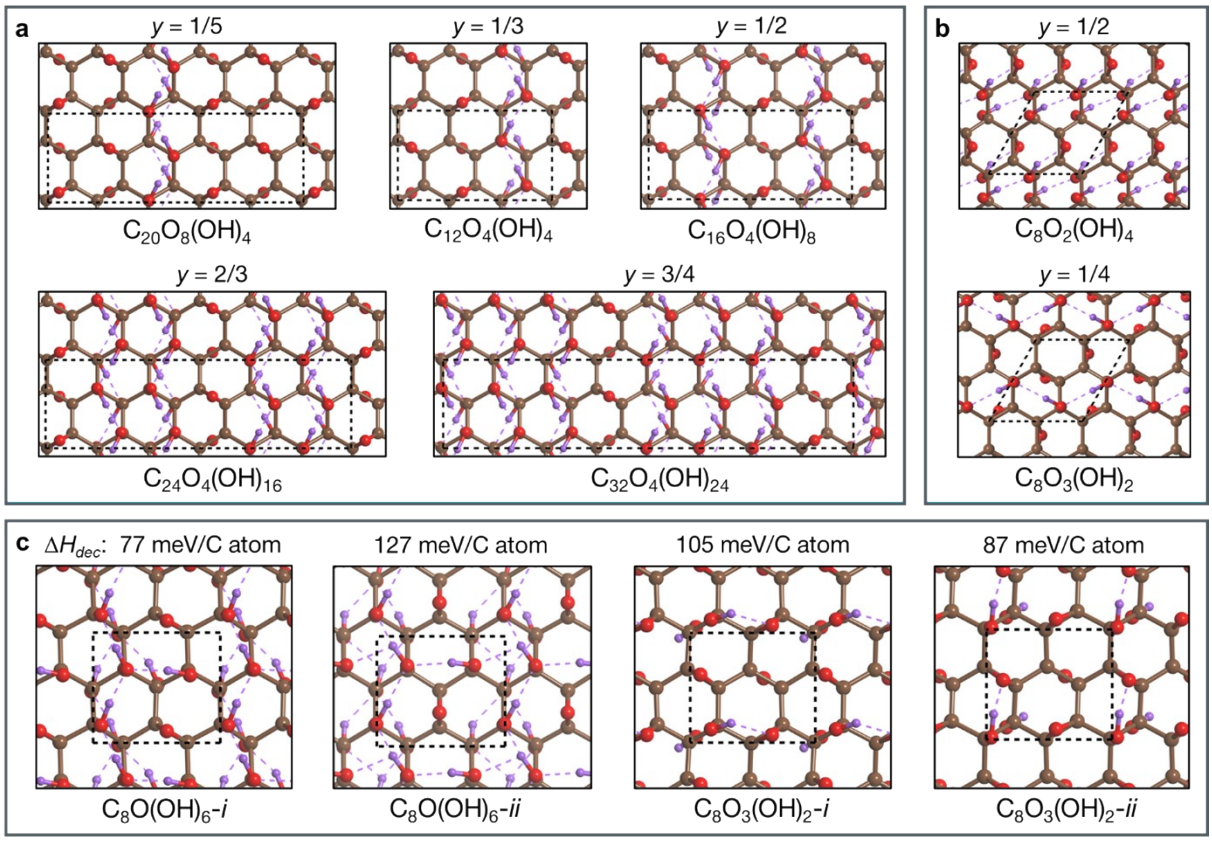

Figure S1. The considered atomic structures of fully oxidized GO with mixed composition. (a) The cut-and-glue GO structures from **Figure 1c**. (b) Low-energy GO structures reported by Guilhon *et al.*[1] (c) Randomly created structures for two GO stoichiometries. The values of decomposition enthalpies ΔH_{dec} calculated via Equation (2) of the main text are given in numbers. Black dashed lines mark the boundaries of the unit cells.

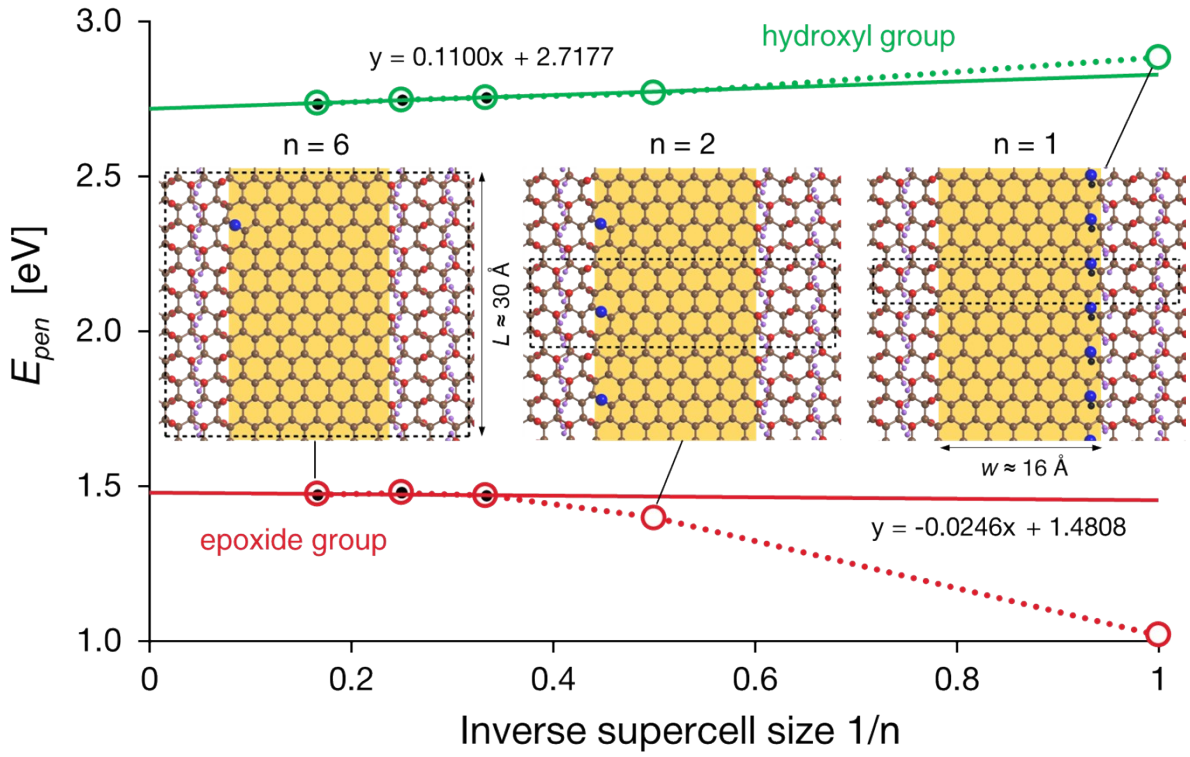

Figure S2. The penalty energy E_{pen} for the movement of epoxide (red points) and hydroxyl (green points) groups as a function of the inverse supercell size. The calculations were conducted at the example of 12-mixed-AGONR' which has both epoxide- and hydroxyl-terminated interfaces with graphene. The supercell width was varied, and the size is measured in multiples n of 12-mixed-AGONR' unit cells. The insets illustrate atomic structure for different supercell sizes (black dashed lines bound the supercells). Displaced oxygen groups (O atoms in blue and H atoms in black) and graphene nanoroad region (yellow filling) are shown in contrast colors for clarity. To obtain the values of E_{pen} for *isolated* oxygen groups, a linear extrapolation (solid lines) to the limit of infinite supercell size ($^{1/n \to 0}$) was made to eliminate the spurious effects of supercell periodicity. The last three points corresponding to n = 3, 4, and 6 were used for fitting.

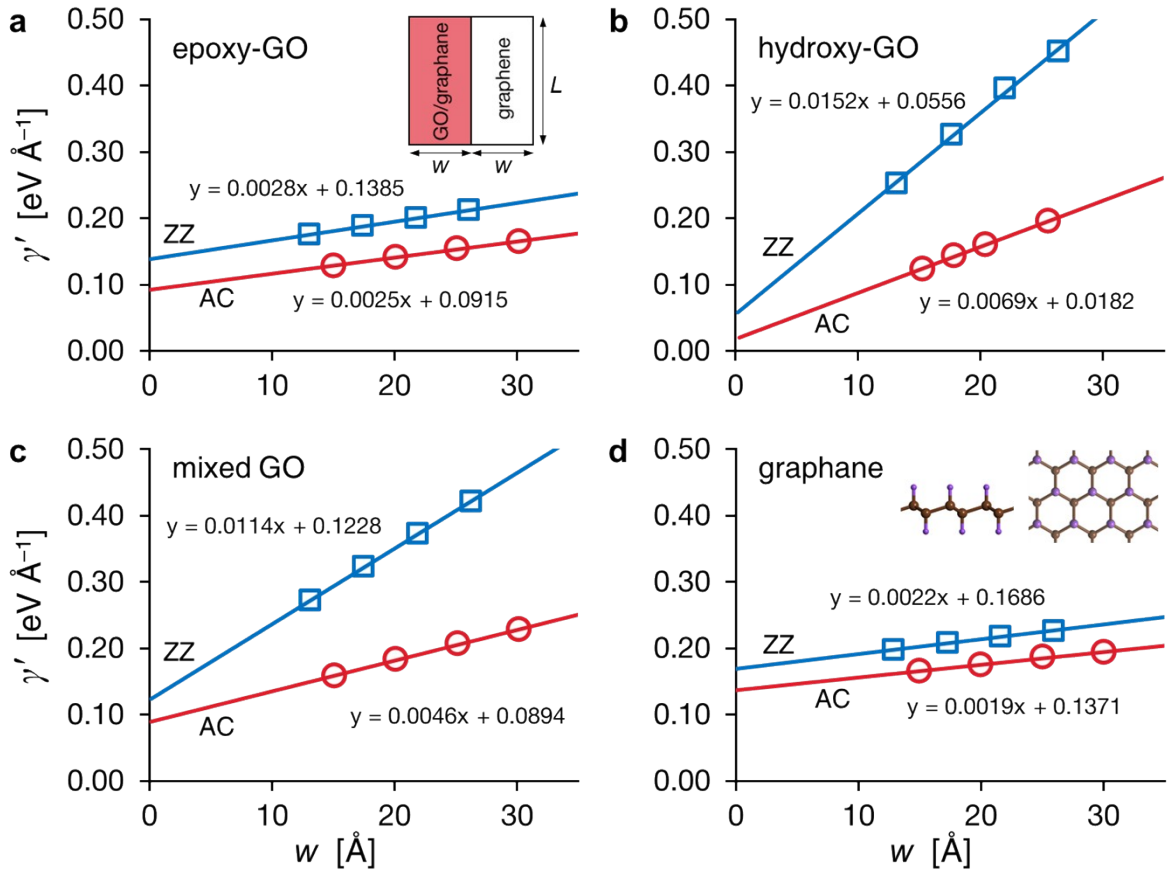

Figure S3. Determination of the GO – graphene interface formation energies γ_{AC} and γ_{ZZ} (in red and blue, respectively). Calculated energy cost due to the interface γ' is plotted vs. the supercell width w (the inset in (a) shows the schematic geometry). Linear least-squares regression performed for the DFT data points (circles and squares) is shown by solid lines and gives the values of γ_{AC} and γ_{ZZ} as an intercept with the y-axis. The panels (a)-(c) correspond to (a) epoxy-GO, (b) hydroxy-GO, and (c) mixed GO. For the comparison, analogous calculations were also carried out for (d) graphane (see the atomic structure in the inset).

To assess the interface formation energies, we adopted the approach introduced by the Yakobson group.[2,3] Normally, the total energy of the supercell contains the contribution from the strain caused by lattice mismatch between the two phases. However, this strain energy scales linearly with the width w of the supercell, and the actual values of interface formation energies γ_{AC} and γ_{ZZ} can be extracted from the DFT data according to the following equation:

$$\gamma'(w) \equiv (E_{tot} - n_{GO}E_{GO} - n_{gr}E_{gr})/2L = (Y\varepsilon^2 w/2 + \gamma_{AC/ZZ}), \quad \text{(S1)}$$

where E_{tot}, E_{GO}, and E_{gr} are the total energy of supercell, the energy of GO and graphene formula units, respectively, with n_{GO} and n_{gr} being the number of these formula units contained in the supercell. On the righthand side, Y and ε are the elastic constant and mismatch-induced strain, respectively. Thus, performing a series of calculations for various w while L is kept fixed it is possible to retrieve γ_{AC} and γ_{ZZ} from the linear fitting procedure, as shown in **Figure S3**.

The obtained results are analyzed in the main text. In addition, we would like only to note that the slopes of the linear dependencies for AC and ZZ interfaces are almost identical in the cases of epoxy-GO and graphane, whereas they are significantly different for mixed and hydroxy-GO. Since from the Equation (S1) the slope is proportional to the elastic constant, this means that epoxy-GO and graphane should have an almost isotropic elastic tensor, and the opposite should be true for mixed and hydroxy-GO.

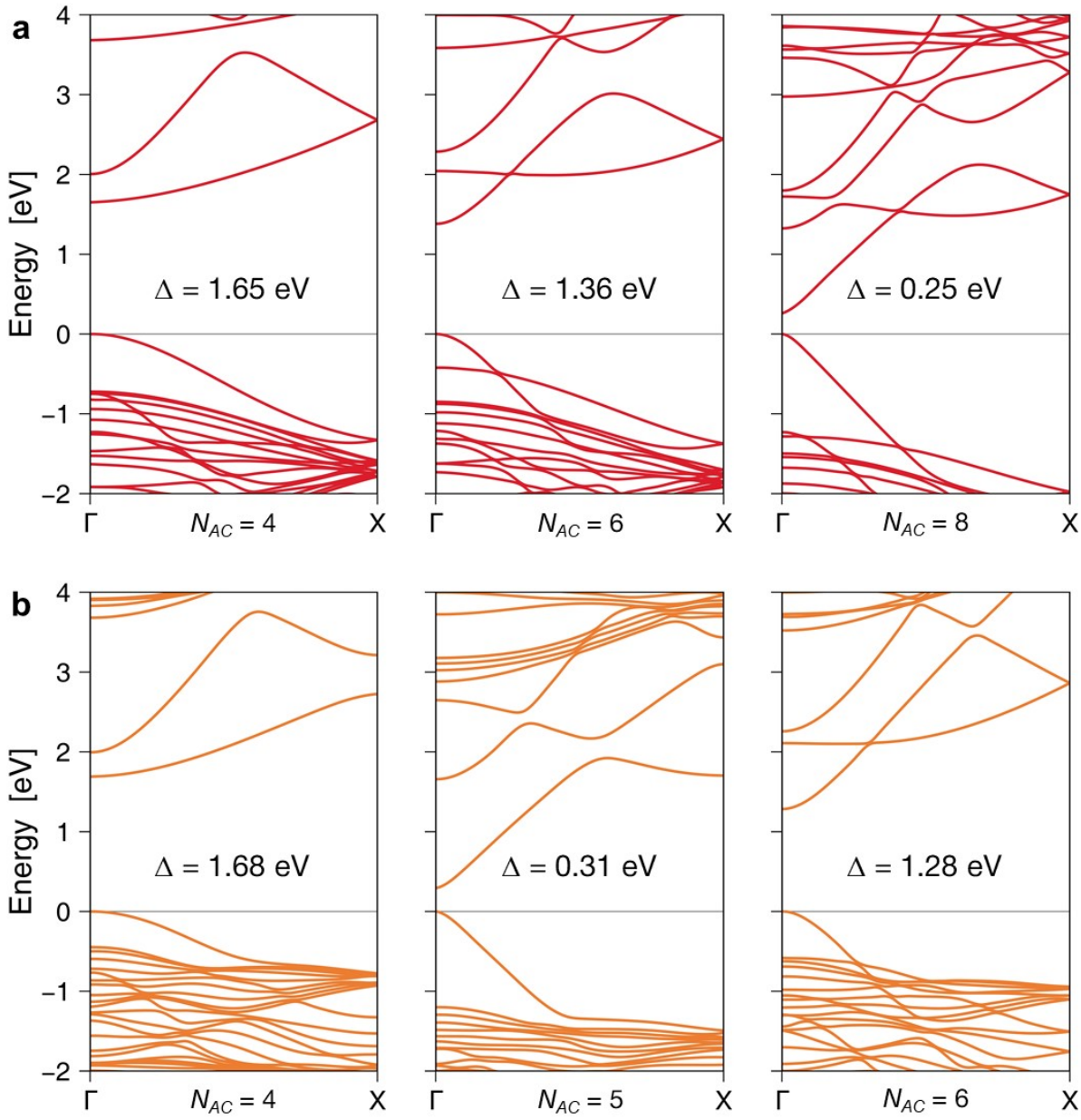

Figure S4. Band structures of (a) epoxy- and (b) mixed-AGONR' of various widths. The widths selected are representatives of three families: $N_{AC} = 3p$, $3p + 1$, and $3p + 2$ (recall that only even N_{AC} are possible in the case of epoxy-AGONR'). Valence band maximum is shifted to zero energy, band gap values are given in the pictures. Note the similarity of band structures for AGONR' of different compositions but belonging to the same width family. Compare also with **Figure 2c** from the main text.

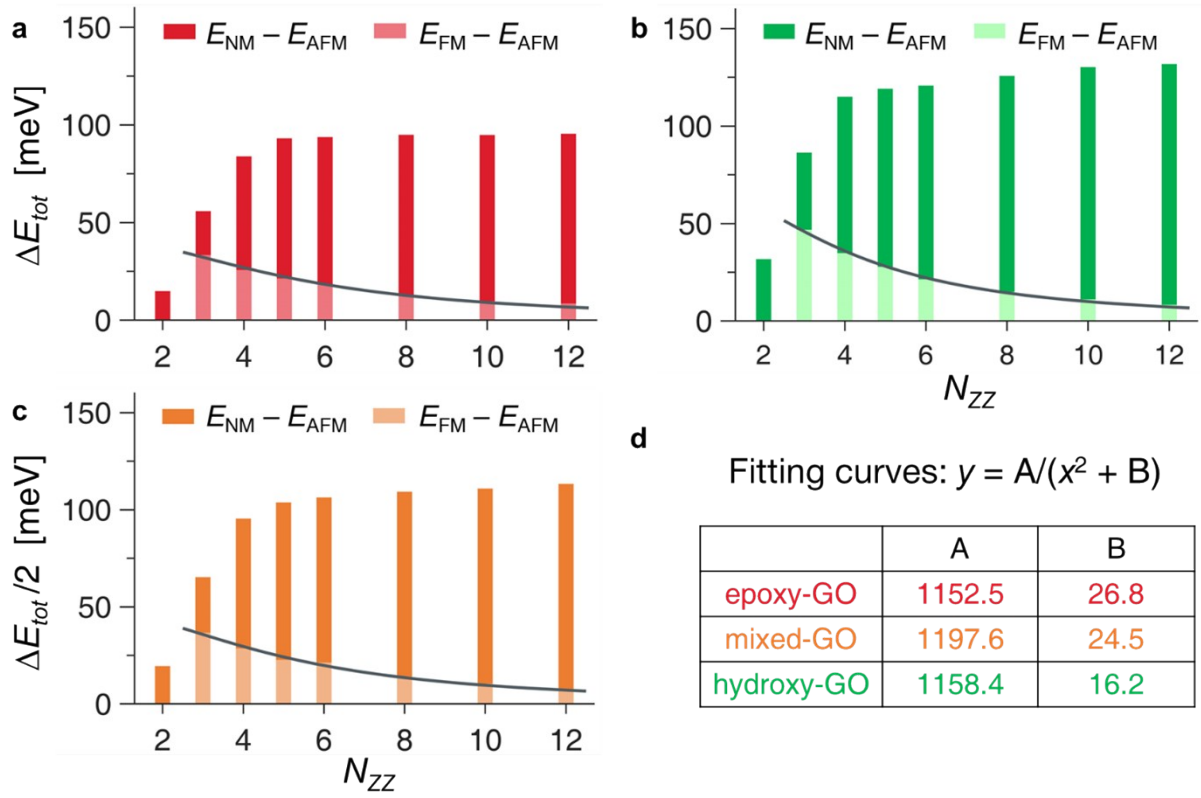

	A	B
epoxy-GO	1152.5	26.8
mixed-GO	1197.6	24.5
hydroxy-GO	1158.4	16.2

Figure S5. (a)-(c) The differences of total energy ΔE_{tot} (per unit cell) between AFM, FM, and NM spin configurations of ZGONR' as a function of a nanoroad width N_{ZZ} for (a) epoxy-GO, (b) hydroxy-GO, and (c) mixed GO. Note that in (c), $\Delta E_{tot}/2$ is plotted to enable the direct comparison between all GO compositions. The energy differences are calculated with respect to AFM configuration as a ground state. Gray solid lines display the fitting of $E_{FM} - E_{AFM}$ energy difference with the inverse square law. (d) The equation used for fitting and the fitted parameters for three GO compositions.

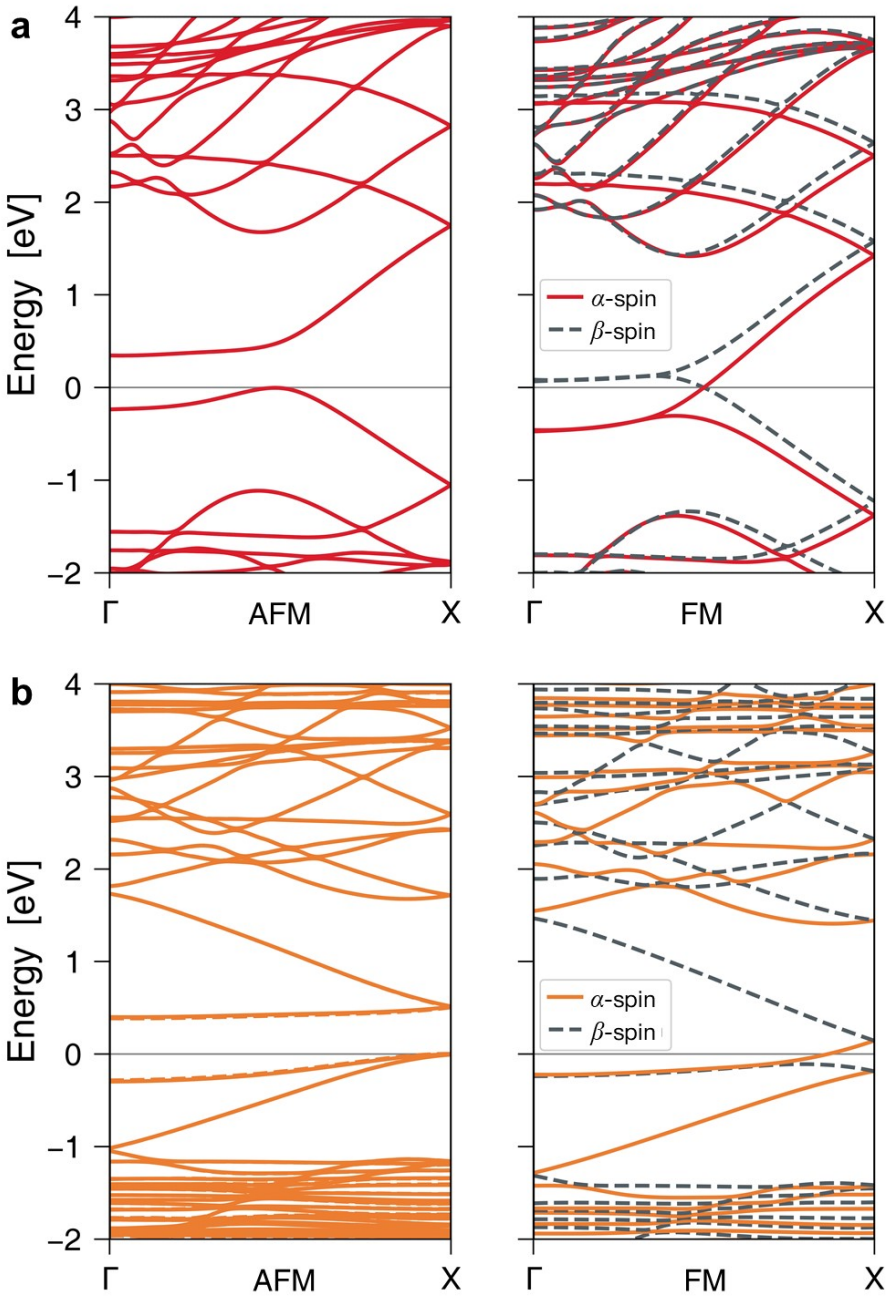

Figure S6. Band structures of 6-ZGONR' in AFM and FM states for (a) epoxy-GO and (b) mixed GO. The valence band maximum is shifted to zero energy. Compare to **Figure 4a** for 6-hydroxy-ZGONR' from the main text. Band structure of 6-mixed-ZGONR' in (b) looks different due to the folding of the Brillouin zone, which is twice smaller for mixed-ZGONR'.

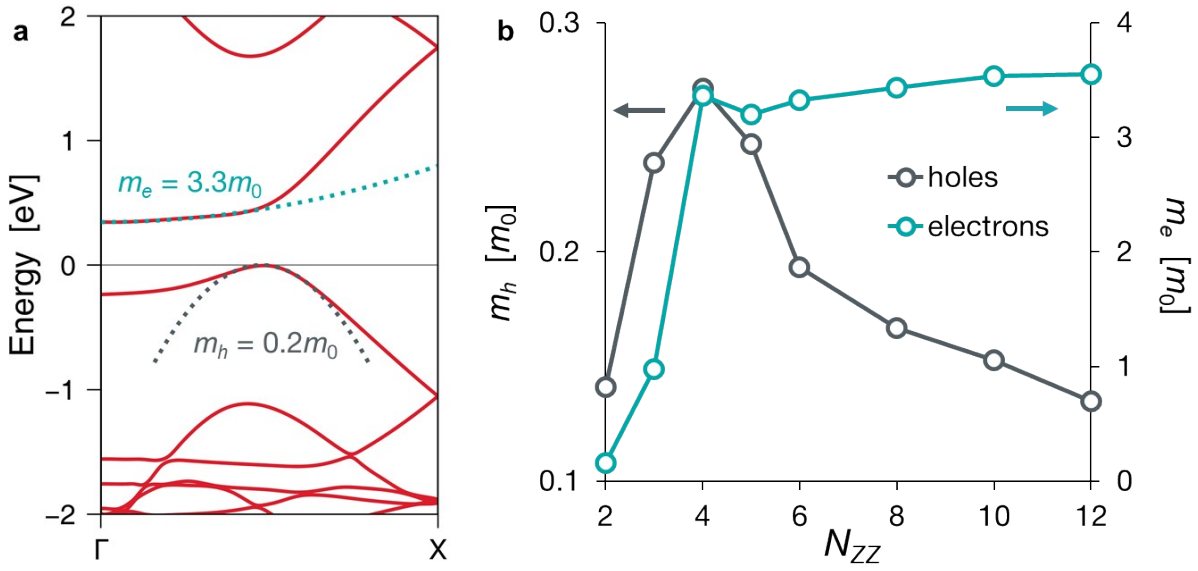

Figure S7. (a) Band structure of 6-epoxy-ZGONR' in AFM state. Dotted lines show parabolic fits used to calculate effective masses. (b) Dependence of the effective masses of electrons and holes in epoxy-ZGONR' on a nanoroad width N_{ZZ}. Note that there are different *y*-axes for electrons and holes.

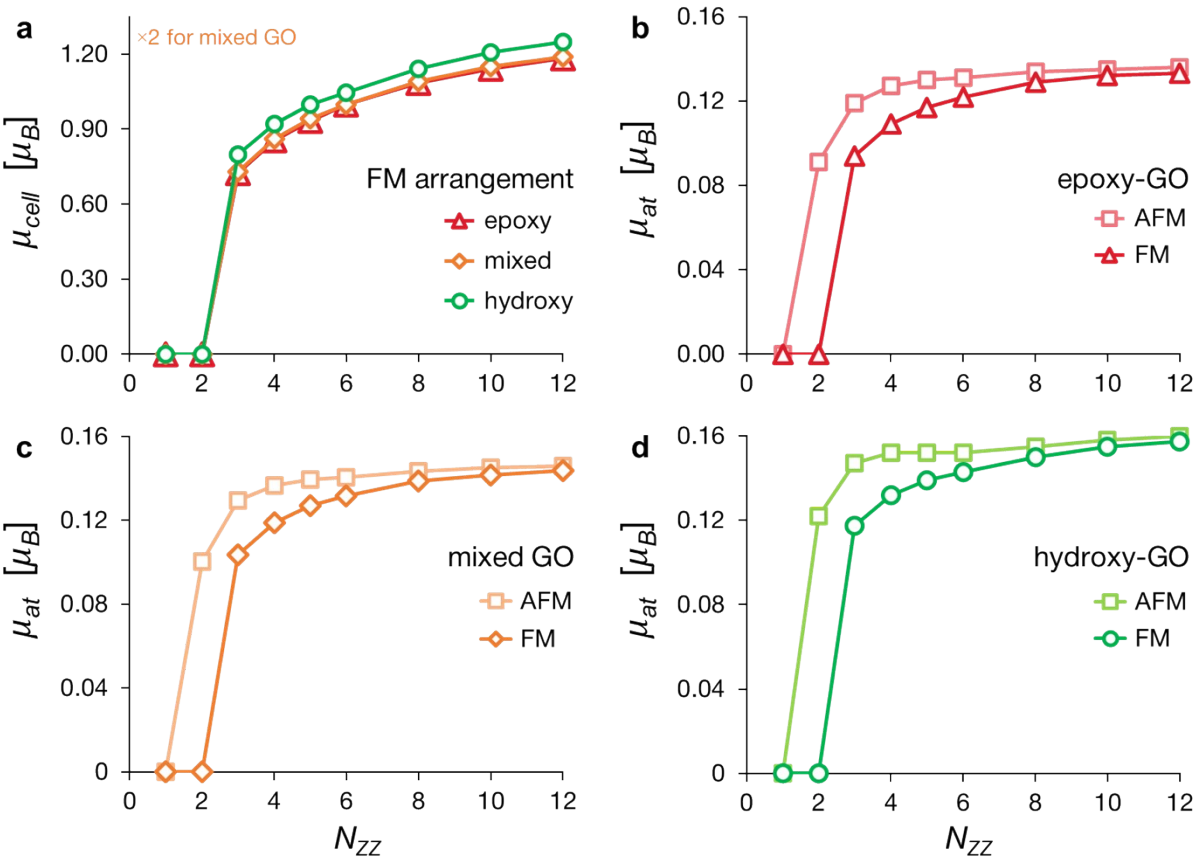

Figure S8. Magnetic properties of ZGONR'. (a) Magnetic moment μ_{cell} per supercell for ZGONR' with the ferromagnetic spin arrangement as a function of a nanoroad width N_{ZZ}. Note that the scale of the *y*-axis is twice bigger for mixed GO (orange line) due to a twice wider supercell. (b)-(d) Local magnetic moments μ_{at} (in μ_B per atom) projected onto the outermost atoms of ZZ nanoroads in AFM (lighter colors) and FM (darker colors) states vs. a nanoroad width N_{ZZ} for (b) epoxy-GO, (c) mixed GO, and (d) hydroxy-GO. The data for AFM states is the same as presented in **Figure 4b** of the main text.

The presented results on the magnetic moment in the ferromagnetic state can be compared to 0.8 μ_B/unit cell for FM nanoroads in graphane[4] and 0.5-0.65 μ_B/unit cell for FM graphene nanoribbons.[5] The higher magnetic moments obtained here for ZGONR' are apparently due to the contribution from oxygen atoms which also manifested some partial spin polarization in our calculations.

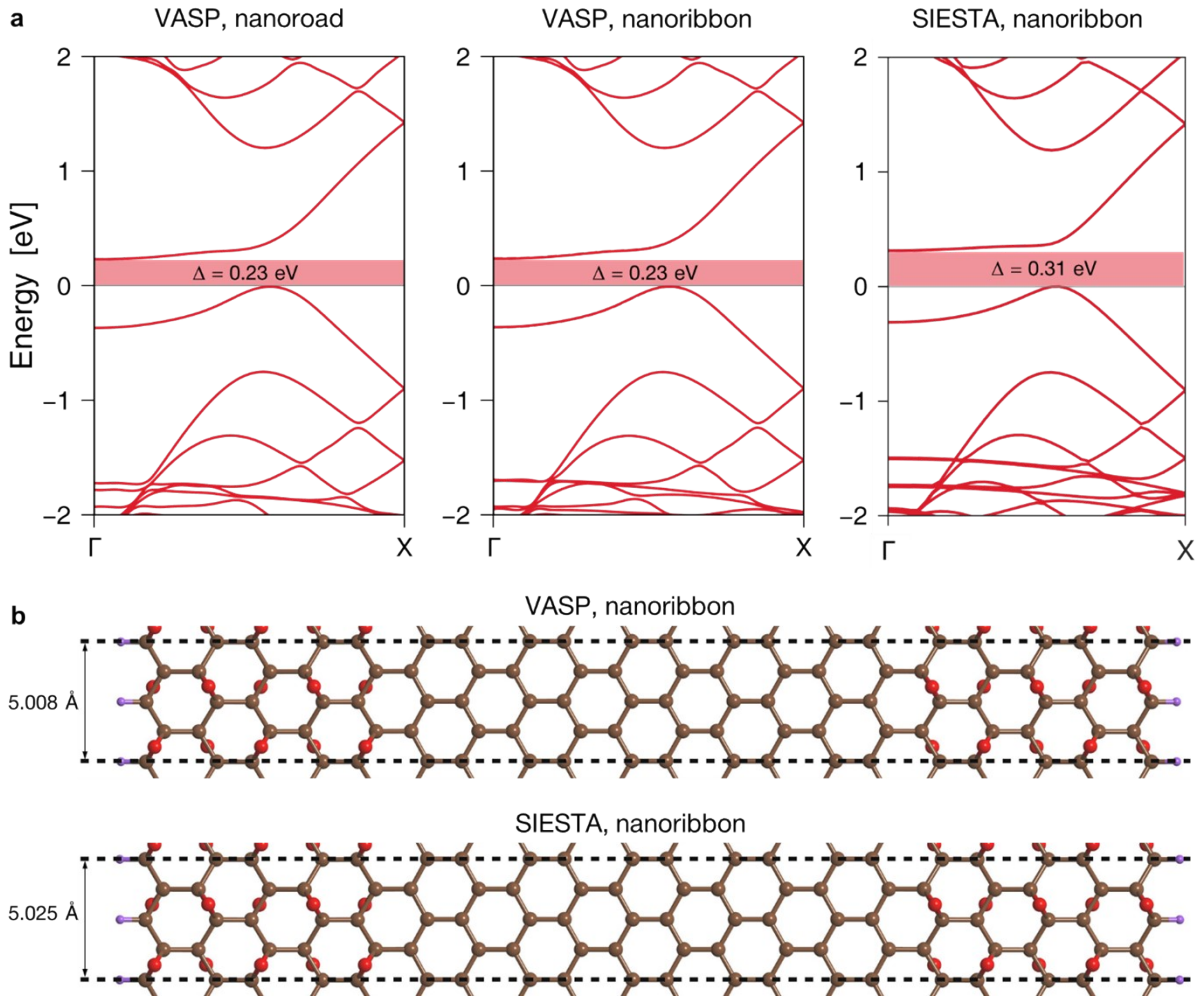

Figure S9. (a) Band structures of 10-epoxy-ZGONR' and the respective nanoribbon calculated using VASP and SIESTA. Band gaps are schematically shown with red filling on band diagrams, with the numerical values given. (b) Atomic structure of the nanoribbon relaxed in VASP and SIESTA. Parameters of the unit cells (shown with dashed lines) in the periodic direction are given for reference.

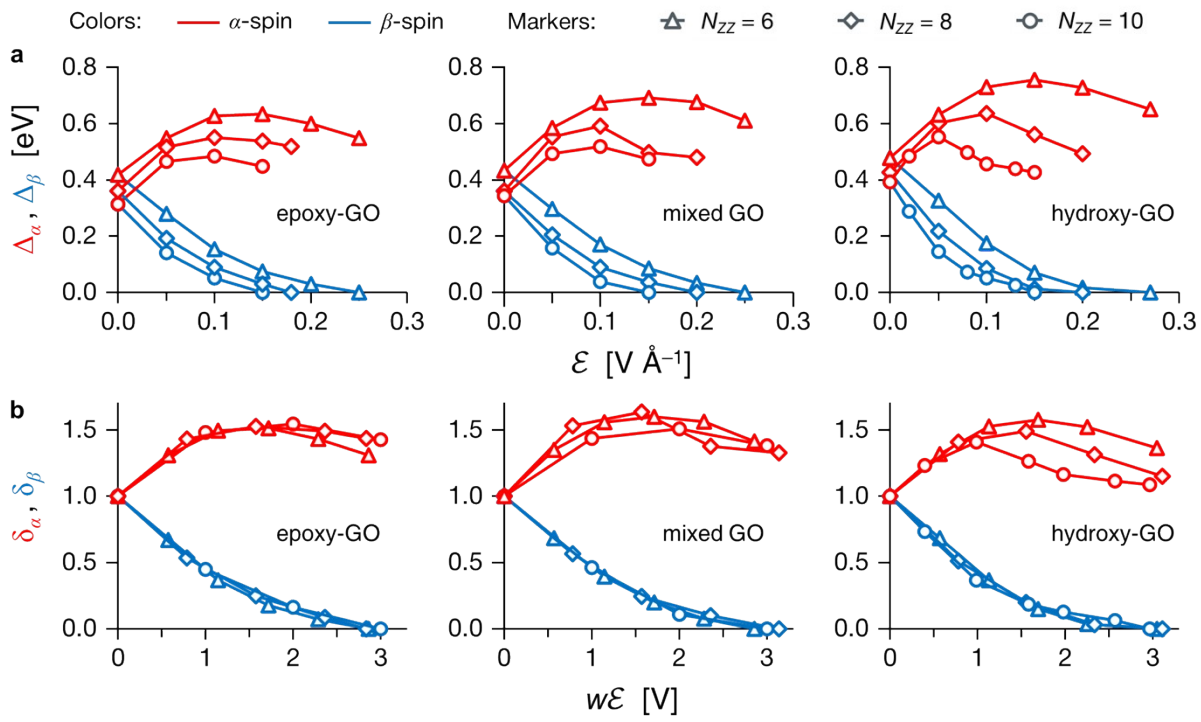

Figure S10. Electric-field-induced half-metallicity of patterned GO. (a) The dependence of band gaps in α- and β-spin channels (Δ_α and Δ_β, respectively) on the external electric field $\mathcal{E}$. (b) The same as **Figure 5d** of the main text but with three GO compositions separated. See the main text for the definition of scaled band gaps δ_α and δ_β. For the interpretation of colors and markers in the figure, please see the legend.

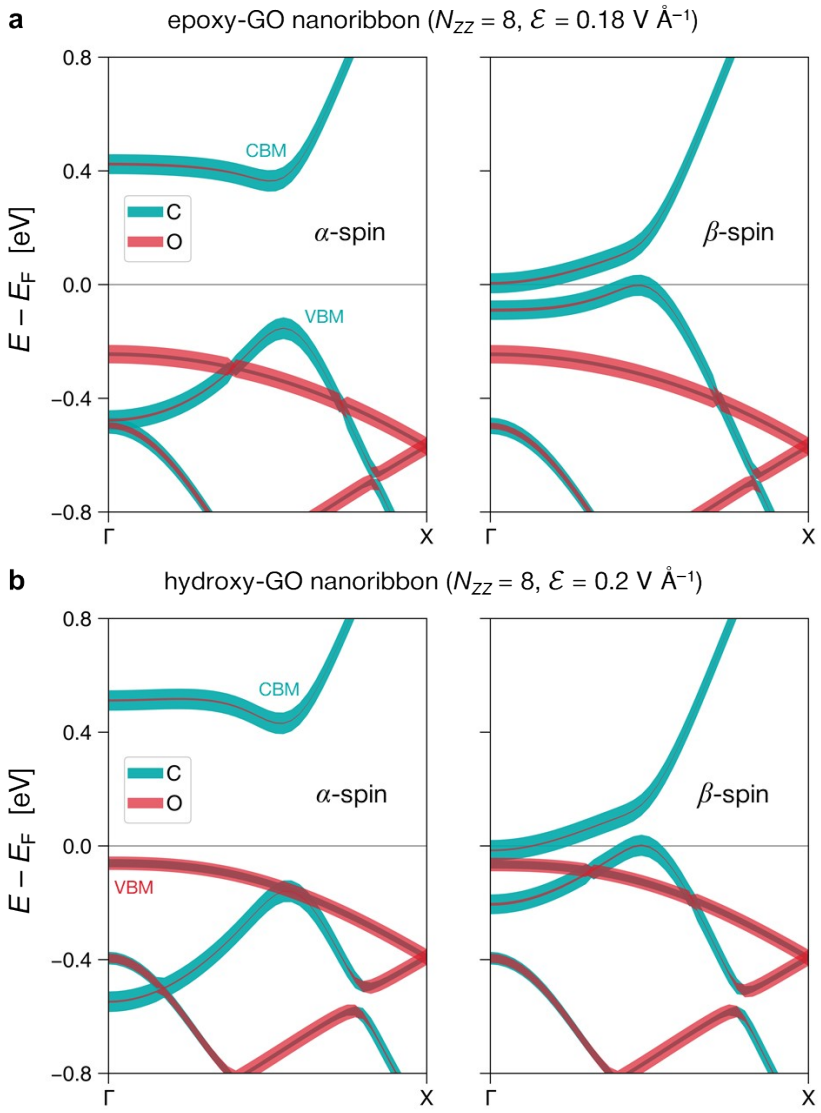

Figure S11. Species-projected band structure of nanoribbons corresponding to (a) 8-epoxy-ZGONR' and (b) 8-hydroxy-ZGONR' in the electric field (the magnitudes are displayed in the figure). For clarity, band structures are plotted separately for α- and β-spin channels, and the contribution from H atoms is not shown. The thickness of lines in the figure is proportional to the contributions from carbon (azure) and oxygen (red) atoms to the respective bands. Fermi energy E_F is set to zero. Bands corresponding to VBM and CBM are marked for the α-spin channel.

As it can be seen, in the case of epoxy-GO both VBM and CBM states are mainly contributed by carbon atoms, whereas in the case of hydroxy-GO the ordering of valence bands is changed and VBM is dominated by the contribution from oxygen atoms. This infers the pure effect of the electric field on the bands of nanoroad and explains the deviation of δ_α from the universal behavior (**Figure S10** and **Figure 5d** of the main text).

References

1 I. Guilhon, F. Bechstedt, S. Botti, M. Marques and L. K. Teles, *J. Phys. Chem. C*, 2017, **121**, 27603–27611.

2 A. K. Singh, E. S. Penev and B. I. Yakobson, *ACS Nano*, 2010, **4**, 3510–3514.

3 S. Bhowmick, A. K. Singh and B. I. Yakobson, *J. Phys. Chem. C*, 2011, **115**, 9889–9893.

4 A. K. Singh and B. I. Yakobson, *Nano Lett.*, 2009, **9**, 1540–1543.

5 L. Pisani, J. A. Chan, B. Montanari and N. M. Harrison, *Phys. Rev. B*, 2007, **75**, 064418.